ROYAL SOCIETY
OF CHEMISTRY

PAPER
Peng Wang, Mohamed Eddaoudi *et al.*
Metal–organic framework-based atmospheric water
harvesting for enhanced photovoltaic efficiency and
sustainability

PAPER

Check for updates

Metal–organic framework-based atmospheric water harvesting for enhanced photovoltaic efficiency and sustainability†

Dalal Alezi, [ID] ‡[a] Renyuan Li, [ID] ‡[b] Norah Alsadun,[cd] Arijit Malik,[c] Osama Shekhah, [ID] [c] Peng Wang [ID] *[b] and Mohamed Eddaoudi [ID] *[c]

The global demand for photovoltaic (PV) cooling is projected to increase over the coming years, driven by the growing adoption of solar energy and the need to improve the efficiency and performance of PV systems. Atmospheric water harvesting-based evaporative cooling (AWH-EC) has the potential to be a key technology for providing sustainable and low-cost cooling. Here, the super-adsorbent Cr-**soc**-MOF-1 is introduced and integrated in a sorption based atmospheric water harvester photovoltaic cooling system. Our results show that the AWH-based cooling component can provide 68.9–136.1 W m^{-2} cooling power, and the temperature of the PV panel can be reduced by ∼10.6–12.6 °C under 0.8–1.1 kW m^{-2} sunlight irradiation. Markedly, the integrated system demonstrates an increase in electricity generation of up to 7.5%. The feasibility of scaling up this cooling strategy is further predicted by simulation, indicating that it is a promising approach to fulfill the cooling demand in the PV industry with broad adaptability.

Introduction

Photovoltaic (PV) technology is considered as one of the most revolutionary approaches that can convert clean and abundant solar energy into electricity. The global newly installed PV capacity reached 268 GW in the year 2022,[1] with the worldwide total installed PV capacity surpassing 1200 GW by the end of the same year, and it is predicted to be more than 3000 GW by 2030.[2] However, PV cells are sensitive to high temperatures due to the increased internal carrier recombination rates of their semi-conductor materials, which is detrimental to solar to electrical energy conversion by PV panels.[3] On the one hand, conversion efficiency loss could be as much as 0.5% at each

degree of temperature increase during operation.[4] On the other hand, the conversion efficiency of a single-junction PV cell is limited to less than 33.3% due to the Shockley–Queisser limit.[5] This limitation results in more than 70% of the total incident sunlight being converted to heat and causes severe heat accumulation on the panels. This heat accumulation not only reduces the electricity generation performance, but also shortens the lifespan of the PV panels.[6]

Water has the highest latent heat of evaporation (*i.e.*, ∼44 kJ mol^{-1}) among all room-temperature liquids.[7] It can be used as a toxic-free green coolant to passively remove heat from hot surfaces through evaporation. The use of water to cool down PV panels has been proposed in the past few years, such as water spray,[8,9] but with limited success in arid or semi-arid regions due to the lack of sufficient liquid water. Additionally, atmospheric water harvesting (AWH) is a process that can extract freshwater directly from air. In fact, there are more than 12 900 billion metric tons of fresh water preserved in air, known as atmospheric water,[10] which can be quickly replenished upon consumption by global water and atmospheric circulation systems driven by solar energy.[11,12] The use of the phase-change process of sorption-based AWH as an alternative cooling approach for heat relocation has gained great interest since 2020.[13,14] The basic working principle of the AWH-based PV panel cooling process can be explained in two steps: the first step is to capture and store water vapor from ambient air as a sacrificial coolant during night when the PV panel is not working, and the second step is to evaporate the stored water

[a] Department of Chemistry, Faculty of Science, King Abdulaziz University, Jeddah, Saudi Arabia

[b] Water Desalination and Reuse Center, Division of Biological and Environmental Science and Engineering, King Abdullah University of Science and Technology, Thuwal 23955-6900, Saudi Arabia. E-mail: peng.wang@kaust.edu.sa

[c] Functional Materials Design, Discovery, and Development Research Group (FMD³), Advanced Membranes and Porous Materials Center (AMPM), Division of Physical Sciences and Engineering (PSE), King Abdullah University of Science and Technology (KAUST), Thuwal 23955-6900, Saudi Arabia. E-mail: Mohamed.eddaoudi@kaust.edu.sa

[d] Department of Chemistry, College of Science, King Faisal University (KFU), Al-Ahsa 31982-400, Saudi Arabia

† Electronic supplementary information (ESI) available: Experimental section describing the synthesis, PXRD, PV panel cooling test, and COMSOL model and simulation. See DOI: https://doi.org/10.1039/d3ma00960b

‡ These authors contributed equally.

to passively relocate waste heat from the PV panels.[13] However, major challenges for its practical applications still remain, including issues such as sorbent capacity and technological adaptability. Therefore, the development of a tailor-made, porous solid—with appropriate structural features and water adsorption properties—is highly desirable. This would be ideal for an energy-efficient atmospheric water harvesting-based evaporative cooling (AWH-EC) process.

Metal–organic frameworks (MOFs) – a versatile class of porous materials comprised of metal nodes or clusters and organic linkers – have shown considerable potential in water adsorption related applications, due to their stability, tunability, and substantial internal voids and surface areas.[15–17] Recently, MOFs like other porous materials have been recently attracting increased interest in many applications like gas storage, sensing catalysis, harvesting water from a low-humidity atmosphere, and controlling the air humidity level by trapping water from a high humidity environment.[18–22] The use of MOFs to improve the performance of PV panels through thermal management and moisture control is a promising and evolving field aiming to enhance the efficiency and applicability of these systems in various environmental and operational scenarios.[23] In a recent study, aluminum-series MOF based thermal batteries have been shown to increase the efficiency of photovoltaic panels by up to 5% through a daytime cooling process driven by water evaporation. They also serve a dual purpose by absorbing water vapor during night-time, which can be effectively integrated into the building's system for regulating humidity. However, the MOF-based thermal batteries for photovoltaic panels still require further development to address challenges such as higher temperature plateaus and to enhance the efficiency of their discharging–charging processes, as well as to balance the material's hydrophilicity and thermal resistance.[22]

Herein, a simple PV panel cooling strategy with broad adaptability from both geological and technological points of view is demonstrated. Cr-**soc**-MOF-1, a hydrolytically stable MOF with a superior water vapor uptake capacity of up to 200% of its own weight,[24] is utilized as a water vapor harvester in the AWH-EC system. In this study, Cr-**soc**-MOF-1 is spray-coated onto a commercially available heat sink to enhance its cooling performance. The MOF-coated heat sink is subsequently attached to the backside of a PV panel, serving as the cooling component.

Our results indicate that the AWH-based cooling component can deliver a cooling power of 68.9–136.1 W m^{-2}, and the temperature of the PV panel can be reduced by 10.6–12.6 °C under 0.8–1.1 kW m^{-2} sunlight irradiation. The cooled PV panel demonstrates a PV electricity generation improvement of up to 7.5%. The feasibility of scaling up this cooling strategy is further predicted by simulation, indicating an almost promising cooling performance.

Results and discussion

Cr-**soc**-MOF-1-coated heat sink preparation

In this study, Cr-**soc**-MOF-1 was chosen to be integrated and evaluated in the atmospheric water harvesting based cooling system due to its distinctive structural, chemical, and water adsorption characteristics.[24] Cr-**soc**-MOF-1 is a highly porous, hydrolytically stable MOF with exceptional water uptake that meets the required criteria for its practical deployment in real water adsorption related applications. It is based on linking trinuclear Cr clusters with 4-connected TCPT^{4-} ligands, which results in a 3-periodic MOF with **soc** topology (Fig. 1a). Cr-**soc**-MOF-1 shows a high water adsorption capacity of 1.95 g (195 wt%) of adsorbed water per gram of sorbent at 75% RH, with an S-shape-like adsorption isotherm (Fig. 1b).

Cr-**soc**-MOF was synthesized on a large scale based on a modified procedure.[24] The purity of the material was confirmed by similarities between the experimental and calculated powder X-ray diffraction (PXRD) patterns (Fig. S2, ESI†). The synthesized Cr-**soc**-MOF was coated on the surface of the heat fins on a commercialized heat sink with a top dimension of 4.5 × 4.5 cm^2 *via* spray coating. The MOF coating was done using a MOF suspension (2.5 mg MOF/1 mL ethanol solvent) that was sonicated for 15 minutes. The suspension was loaded into a 100 mL
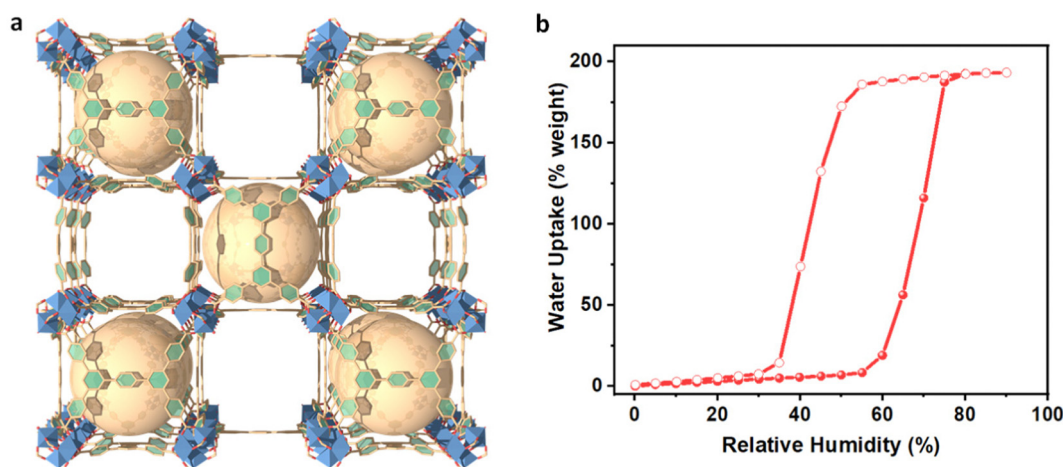

Fig. 1 (a) Crystal structure of Super-adsorbent Cr-**soc**-MOF-1. (b) Water sorption isotherm at 298 K for activated Cr-**soc**-MOF-1.

plastic sprayer and the MOF suspension solution was promptly sprayed onto the heat fins for 30 seconds in each cycle, which were subsequently dried under ambient conditions for 2 minutes. The spraying and drying process was repeated until desired loading weight of the MOF was achieved (see Fig. S1, ESI†). The MOF-coated heat sink exhibited very good distribution and adhesion to the heat fins as revealed by the scanning electron microscopy images (Fig. 3). The MOF-coated heat sink was directly attached to the backside of a 5.0×5.0 cm^2 commercialized PV panel (SUNTHING GOOD Co. Ltd) that was pasted with thermal grease to ensure close contact and reduce heat resistance across the boundaries between the PV panel and heat sink (Fig. 2b) and assembled with the device for testing (Fig. 2c).

PV panel cooling performance. The PV panel cooling test was performed under simulated sunlight and lab conditions to compare the cooling efficiency of the Cr-**soc**-MOF-1-coated heat sink at various sunlight intensities. The surface temperature of PV panels was used as the direct indicator of the cooling performance. The PV characteristics including open circuit voltage (V_{oc}), efficiency, and maximum power output (P_{max}) were calculated and compared based on the current–voltage (I–V) curves obtained from the source meter. The prototype device with the Cr-**soc**-MOF-1-coated heat sink worked in the diurnal mode. Water vapor adsorption was conducted during night when the PV panel was not working, while the evaporative cooling process, also called the MOF regeneration process, was performed during the daytime driven by waste heat from the PV panel.

The equilibrium surface temperature of the PV panel at different sunlight intensities is displayed in Fig. 4a–d. As seen, when without any cooling measurements under 0.8, 0.9, 1.0, and 1.1 kW m^{-2} sunlight irradiation, the PV temperatures were measured to be 56.7, 58.2, 61.5, and 63.1 °C, respectively. When a heat sink was applied, the surface temperature of the PV panel could be reduced by ~8.5–11.5 °C, which could be attributed to the strengthened heat dissipation process through the significantly enlarged cooling surface area of the heat sink.

As a proof-of-concept, when the heat sink was coated with a layer of MOF, the PV temperatures could be further reduced by 2.3, 2.2, 1.6, and 1.1 °C, respectively, which was owing to the evaporative cooling process of water in the MOF layer. Fig. 4e displays the IR images of the PV panel under different test conditions. Clear contrast differences could be observed across the sunlight intensities of 0.8–1.1 kW m^{-2} and under different cooling configurations such as without cooling, heat sink cooling, and Cr-**soc**-MOF-1-coated heat sink cooling, demonstrating their distinctive temperature differences.

The amount of water evaporated for cooling during the test was determined by the mass change (profiled in Fig. 5a) of the prototype device with the Cr-**soc**-MOF-1-coated heat sink. The slope of the mass change curves and the final weight loss reflected the water evaporation rate during the test, which highly depended on the incident sunlight intensity. During the 120-min test, the mass changes due to water evaporation at 0.8, 0.9, 1.0, and 1.1 kW m^{-2} sunlight intensities were 0.41, 0.56, 0.63, and 0.81 g, respectively. The averaged evaporative cooling power provided by the Cr-**soc**-MOF-1 layer was calculated based on eqn (1):

$$P_{MOF} = \frac{\Delta H_{vap} \times m_{water}}{A \times t} \quad (1)$$

where ΔH_{vap} and m_{water} are the enthalpy of vaporization (2450 J g^{-1}) and mass change (g) of water, A is the surface area of the PV panel in contact with the Cr-**soc**-MOF-1-coated heat sink (20.25 cm^2), and t is the test time (7200 s). Therefore, the cooling power values contributed by the MOF layer at 0.8, 0.9, 1.0, and 1.1 kW m^{-2} were calculated to be 68.9, 94.1, 105.9, and 136.1 W m^{-2}, respectively (Fig. 5b). Such cooling power enhancement *via* evaporative cooling is compatible with or even higher than that of the radiative cooling power (*i.e.*, 68–136 W m^{-2} *vs.* 40–120 W m^{-2}), demonstrating its broad potential in fulfilling different cooling demands.

The PV cooling test performed under standard illumination at the absolute air mass of 1.5 (AM 1.5) and at 1.0 kW m^{-2} sunlight intensity was further extended to 7 hours to test the durability of the cooling layer within each working cycle
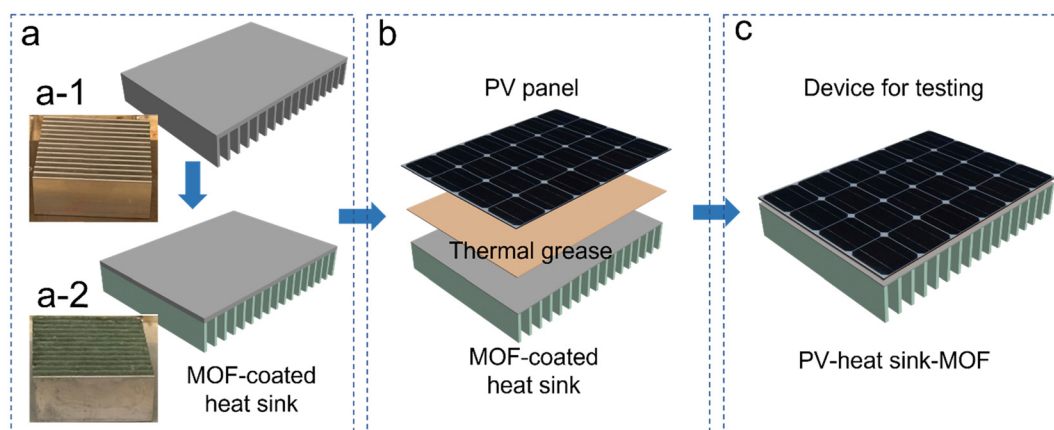

Fig. 2 Schematic of device assembly processes. (a) the MOF coating process; (a-1) photo of the heat fins before spray coating; (a-2) photo of the heat fins after spray coating with Cr-**soc**-MOF-1. (b) The device assembling process. (c) The as-assembled devices for testing.
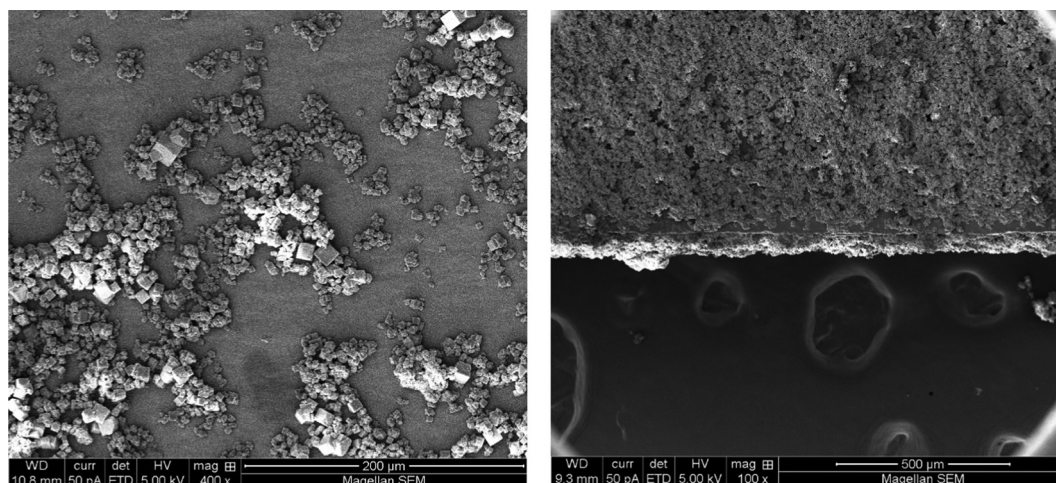
Fig. 3 Top-view SEM images of the Cr-**soc**-MOF-1 particles as-synthesized (left) and after the spray coating process on the heat fins (right).
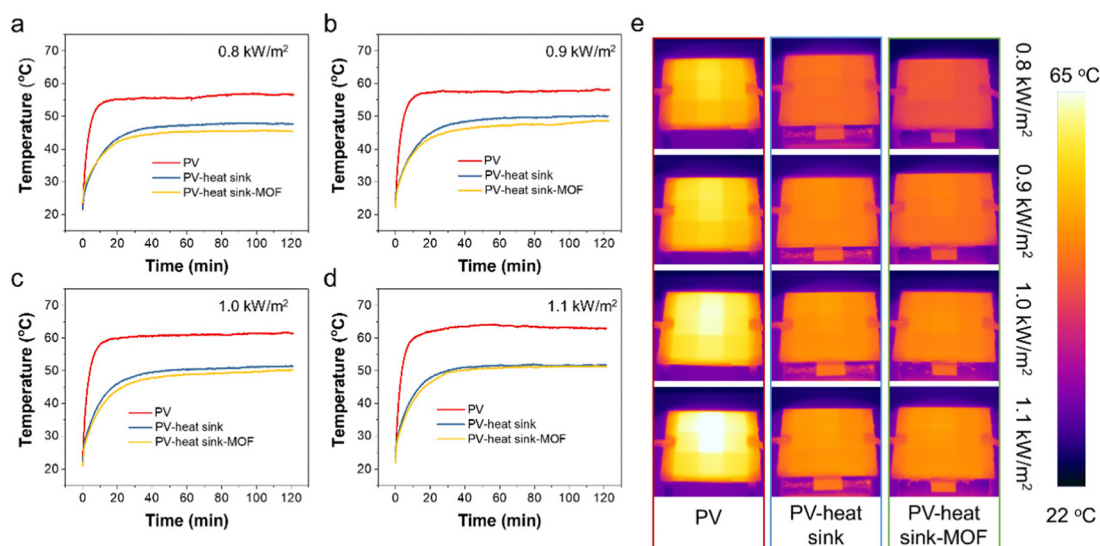

Fig. 4 The temperature change of PV panels with different device configurations at different sunlight intensities. (a)–(d): 0.8, 0.9, 1.0, and 1.1 kW m^{-2}, respectively. (e) IR images of the PV panel under different conditions.

(Fig. 5c). As seen, the mass change curve at the first 4 hours shows a nearly linear relationship along with time elapse, with the evaporated water weighing 1.1 g. Then the slope of the mass change curve drastically decreased and plateaued after approximately 2 extra hours of test. The rapid increase of the temperature in the first 1 h is mainly due to the heat accumulation at the surface of the PV panel before the balance between heat generation and heat dissipation is achieved. With increase in the panel temperature, the cooling power of heat radiation, convection, and the evaporative cooling power by water desorption of the water-saturated MOFs are enhanced, and thus showing a mitigated temperature increase rate. The final mass change was 1.3 g, and the plateaued curve indicated the exhaustion of adsorbed water in the Cr-**soc**-MOF-1 cooling layer. The temperature change profile displays a huge jump within the first hour from a room temperature of $\sim$22.5 °C to

$\sim$48.5 °C and then a slow increase to 51.4 °C until 6 hours of test. The final temperature was observed to be 52 °C at the 7th hour, showing a 0.6 °C increase after the exhaustion of water in the Cr-**soc**-MOF-1 cooling layer. Fig. 4d shows the IR images of the PV panel at different time nodes and their contrast change indicates the inclining of the PV panel surface temperature.

The characteristics of the PV panel during the test, including V_{oc}, efficiency, and P_{max}, were calculated from the I–V curves obtained using a Keithley 2400 source meter under different solar strengths and device configurations (Fig. 5). The V_{oc} of the pristine PV panel without cooling was quickly dropped from 5.7–5.75 V to 5.05–5.15 V within the first 20 min at different sunlight intensities. When the heat sink was applied, the V_{oc} changed from 5.7–5.75 V to 5.3–5.35 V within the first 20 min and remained constant at around 5.3 V until the end of the test. When the Cr-**soc**-MOF-1-coated heat sink was applied, the V_{oc}
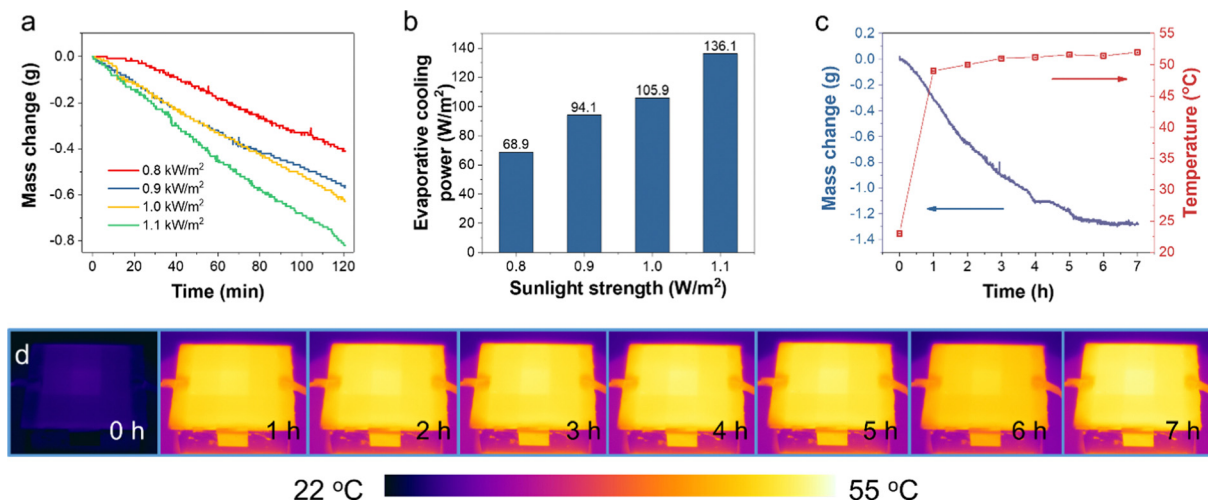
Fig. 5 The cooling performance of the Cr-**soc**-MOF-1-coated heat sink at different sunlight intensities. (a) The mass change of the MOF during the test. (b) The calculated evaporative cooling power was contributed by the evaporation of water from the MOF. (c) The mass change of the MOF and the temperature change of the PV panel in a prolonged 7-hour cooling test. (d) The IR images of the PV panel at different time nodes.

drop was further delayed, and the equilibrium V_{oc} was ~ 0.05 V higher than that of the heat sink without the coating and ~ 0.25–0.3 V higher than that of the pristine PV panel, indicating the strengthened cooling effect due to the MOF coating (Fig. 6a–d).

Similarly, the efficiency of the PV panel shows a similar trend to that of the V_{oc} change. The PV panel cooled by the MOF-coated heat sink demonstrated the highest efficiency,

followed by the PV panel cooled by a pristine heat sink and then the pristine PV panel without any cooling (Fig. 6e–h). The equilibrium efficiencies at 0.8, 0.9, 1.0, and 1.1 kW m^{-2} sunlight intensities were 12.3%, 12.2%, 11.8%, and 11.3% for pristine PV, 12.9%, 12.5%, 12.3%, and 12.0% for the PV panel cooled by the heat sink, and 13.2%, 12.9%, 12.6%, and 12.2% for the PV panel cooled by the Cr-**soc**-MOF-coated heat sink, respectively. It should be mentioned that the original efficiency
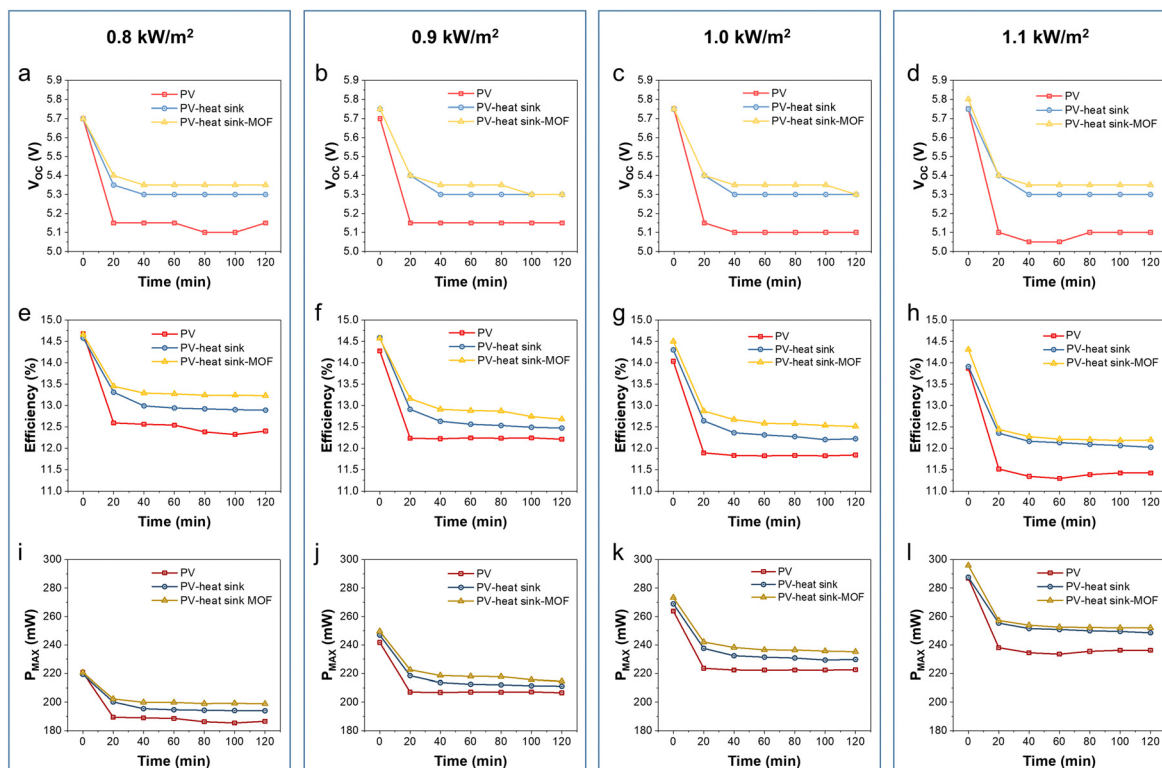

Fig. 6 The PV characteristics under different device configurations and at different sunlight intensities. (a), (e) and (i): 0.8 kW m^{-2}. (b), (f) and (j): 0.9 kW m^{-2}. (c), (g) and (k): 1.0 kW m^{-2}. (d), (h) and (l): 1.1 kW m^{-2}.

of the PV panel should be ∼14.8%, and the initial efficiency differences of the PV panel at different sunlight intensities among the three different device configurations were because of the heating effect of the PV panel during its first I–V curve collection under sunlight irradiation.

The P_{max}, which serves as the indicator of the electricity generation ability of the PV panels at an optimized load, is also compared in this work (Fig. 6i–l). At the sunlight intensities of 0.8, 0.9, 1.0, and 1.1 kW m^{-2}, the P_{max} of the pristine PV panel without cooling rapidly dropped from 219.3, 241.7, 263.8, and 286.9 mW to 185.3, 207.0, 221.4, and 237.5 mW, respectively. The PV panel cooled with the heat sink showed a delayed P_{max} decline from 220.6, 246.9, 268.8, and 287.6 mW to 193.9, 211.1, 229.4, and 249.5 mW, respectively. For the PV panel cooled with the Cr-**soc**-MOF-coated heat sink, the P_{max} slowly dropped from 220.7 to 199.2 mW (0.8 kW m^{-2}), 249.6 to 220.1 mW (0.9 kW m^{-2}), 273.3 to 235.2 mW (1.0 kW m^{-2}), and 295.8 to 251.8 mW (1.1 kW m^{-2}), showing the highest P_{max}, among others. The P_{max} increments were estimated to be ∼7.5, 6.3, 6.2, and 6.0%, respectively. Thus, the Cr-**soc**-MOF coating can further strengthen the heat dissipation process during the PV panel cooling, thereby promoting the performance of the PV panel at different sunlight intensities.

The first data point of the PV panel cooled by the Cr-**soc**-MOF-coated heat sink in both efficiency and P_{max} displays a distinctive higher value at 1.0 and 1.1 kW m^{-2} sunlight intensity, indicating a delayed thermal-induced heating effect of the PV panel under strong sunlight irradiation. Notably, even though the evaporative cooling power was calculated to be the highest among others at 1.1 kW m^{-2}, both the efficiency and P_{max} observed for the Cr-**soc**-MOF-coated heat sink batch were close to those of the pristine heat sink batch with less than 2% of enhancement in both cases. This is because the waste heat generated by the PV panel at high sunlight intensity induces a stronger thermal effect, which facilitates the evaporation of water from the MOF layer, reflected as the rapid mass change in the referred test (Fig. 5a). However, upon the loss of water, a higher temperature is required to further remove the residual water inside the MOF that has a stronger affinity, and thus the equilibrium MOF temperature increases, leading to a reduced efficiency and P_{max} of the attached PV panel due to high temperature. Based on the observed V_{oc}, efficiency, and P_{max} under different test conditions, it is clear that the cooling strategies by using either the heat sink or the heat sink coated with MOFs are more effective at a sunlight intensity of 1.1 kW m^{-2}, with the MOF-coating strategy successfully enhancing PV panel performance compared to the pristine heat sink. Such a phenomenon indicates that appropriate cooling under strong sunlight irradiation is necessary, further demonstrating the effectiveness of the MOF coating in strengthening PV panel performance. It is also worth to mention that the structural stability of the material is completely maintained after these tests, as confirmed by PXRD (Fig. S3, ESI†). Furthermore, a comparison of electricity generation improvement using AWH-based cooling materials is summarized in Table S1, ESI.†

Prediction of PV panel cooling performance at the enlarged scale. To investigate the feasibility of the cooling strategy at the enlarged scale and demonstrate its potential for fitting the industrial cooling demands, simulation-based performance prediction was conducted using the COMSOL Multi-physics model.

In the case of a Cr-**soc**-MOF-coated heat sink, both the heat and mass transfer processes are considered the determining factors of the evaporation of water from the MOF layer. Since the conductive heat transfer is insignificant due to the small temperature differences between the PV panel or MOF layer surfaces and the surrounding ambient, it is not considered in the modeling process. The heat balance in the model is described as follows:

$$P_{in} = P_{rad,PV} + P_{con,PV} + P_{rad,MOF} + P_{con,MOF} + \Delta H_{vap} \cdot f_{evap} \tag{2}$$

where P_{in} is the total heat generated by the PV panel during operation (W) and $P_{rad,PV}$, $P_{con,PV}$, $P_{rad,MOF}$, and $P_{con,MOF}$ are the energy exchange power (W) by radiation and convection across the PV panel top surface and the MOF layer surface, respectively. ΔH_{vap} is the desorption heat of water from the MOF layer, which is approximated to be the evaporation enthalpy of water (J g^{-1}) in the simulation. f_{evap} is the vapor flux (g s^{-1}). The radiative heat transfer can be described by the Stefan–Boltzmann law, as shown in eqn (3).

$$P_{rad} = A\varepsilon\sigma(T_s^4 - T_{amb}^4) \tag{3}$$

where A is the surface area (m^2) of the PV panel or the MOF layer. ε is the Stefan–Boltzmann constant and σ is the emissivity of the PV panel or the MOF layer (W m^{-2}k). T_s and T_{amb} are the surface temperatures (K) of the PV panel and MOF layer, and the ambient temperature (K), respectively. The convective heat transfer can be calculated using:

$$P_{con} = \rho C_p \frac{\partial T}{\partial t} + \nabla \cdot (-k\nabla T) + \rho C_p \cdot u \cdot \nabla T \tag{4}$$

where ρ is the density of air (g m^{-3}), C_p is the specific heat capacity of air (J g^{-1} K^{-1}), T is the temperature (K), t is the time (s), k is the thermal conductivity of air (W m^{-2}K), ∇T is the temperature gradient between the PV panel surface or MOF layer surface and the surrounding ambient, and u is the air velocity by natural convection (m s^{-1}).

The MOF layer is considered as a porous medium and the total amount of water in the MOF layer (W_{total}) can be expressed as:

$$W_{total} = \varphi_p s_l \rho_l + \varphi_p s_g \rho_g \omega_v \tag{5}$$

where φ_p is the porosity of the MOF layer and s_l, s_g, ρ_l, and ρ_g are the saturation variables and densities (g m^{-3}) of liquid water and water vapor, respectively, with $s_l + s_g = 1$. ω_v is the water vapor mass fraction, defined as:

$$\omega_v = \frac{M_v \cdot RH \cdot C_{sat}(T)}{\rho_g}$$

where M_v is the molar weight of water vapor (g mol^{-1}), RH is the relative humidity (%), and $C_{sat}(T)$ is the saturated water concentration (mol m^{-3}) at temperature T. The time-dependent f_{evap} can be expressed as:

$$f_{evap} + \rho_g u_g \cdot \nabla \omega_v + \nabla g_w + u_l \cdot \nabla \rho_l + \nabla g_{lc} = 0 \qquad (6)$$

The convection of water vapor is governed by the total pressure gradient within the flow field u_g and is calculated using the Brinkman equation. g_w is defined as the binary diffusion of dry air and water vapor in the gaseous phase:

$$g_w = -\rho_g D \nabla \omega_v \qquad (7)$$

where D is the diffusivity ($m^2\ s^{-1}$) of water vapor in the MOF layer.

The water velocity u_l ($m\ s^{-1}$) is calculated using Darcy's law:

$$u_l = -\frac{k_l}{\mu_l} \nabla p_g \qquad (8)$$

where k_l is the permeability of liquid water (m^2), u_l is the viscosity (Pa s^{-1}) of liquid water, and p_g is the pressure distribution of moist air in the MOF layer.

The capillary transportation of liquid water g_{lc} is defined as:

$$g_{lc} = -D_w \frac{\partial W_{total}}{\partial RH} \nabla RH \qquad (9)$$

with D_w being the diffusion coefficient of water due to the capillary effect.

In the first place, a small-scale cooling model was executed with the defined working conditions the same as the lab conditions under which the PV panel-cooling test was performed. The calculation results indicated that the temperature at the equilibrium state is close to the experimental data, which demonstrated the accuracy of the model (Fig. 7a and c). Then, the model dimension was further scaled up to $1 \times 2\ m^2$ to predict the cooling effect using the same strategy (Fig. 7b). The wind speed was assumed to be 1 m s^{-1} and the ambient temperature was set to 30 °C. The P_{in} was found to be 1600 W, which is equal to 800 W m^{-2} based on the assumption that 20% of the total incident solar energy is converted to electricity or reflected at 1000 W m^{-2} sunlight intensity. As seen in Fig. 7d, the equilibrium temperature is calculated to be ∼52 °C, which is slightly higher than that of the small scale (*i.e.*, 48 °C) due to the reduced wind speed across the larger dimension beneath the PV panel. However, this temperature is still much lower than that of the pristine PV panel simulated under the same conditions (*i.e.*, 61 °C, Fig. 7e). The simulation results successfully demonstrated the great potential of the cooling strategy on the enlarged scale, indicating that it provides a possible solution to solve the industrial cooling demands in a sustainable manner.

In conclusion, this work introduces a new AWH-based PV panel cooling strategy based on water vapor sorption using MOFs that can be easily applied on both the deployed and the new PV panels. In this study we have deployed the super-adsorbent Cr-**soc**-MOF-1 in a sorption based atmospheric water harvester photovoltaic cooling system. The results demonstrate that the AWH-based cooling component can provide 68.9–136.1 W m^{-2} cooling power, and the temperature of the PV panel can be reduced by ∼10.6–12.6 °C under 0.8–1.1 kW m^{-2} sunlight irradiation. Markedly, the integrated

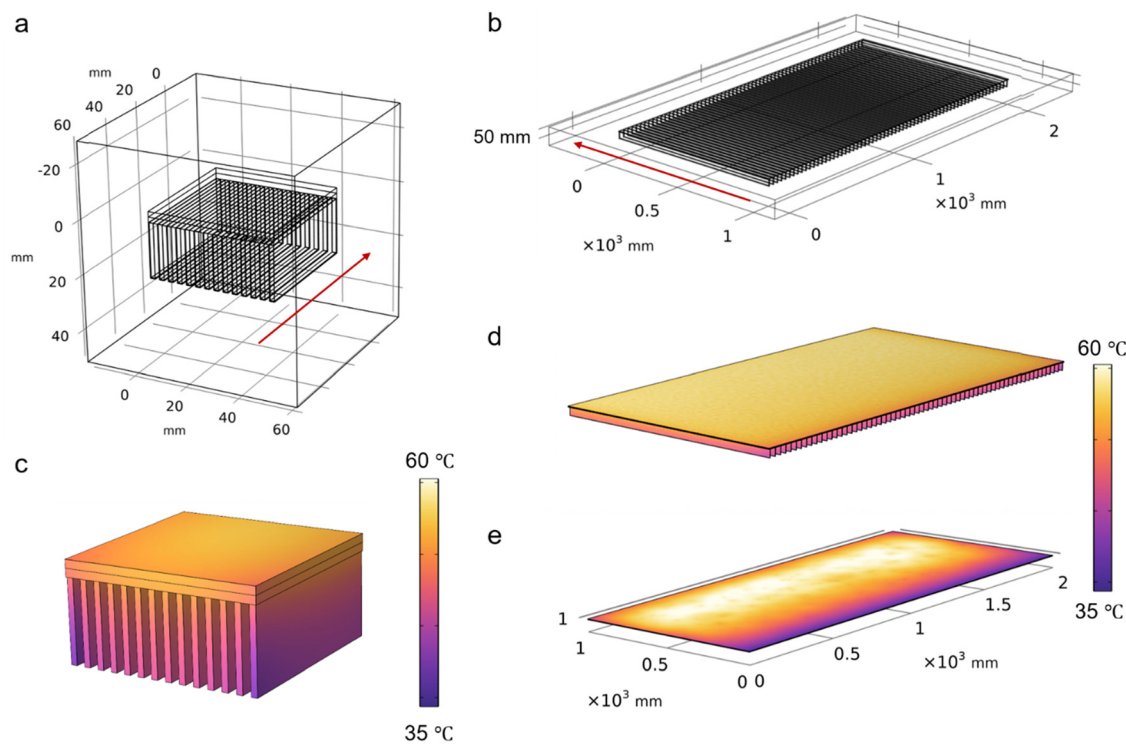**Fig. 7** COMSOL simulation of PV panel cooling effects at different dimensions. (a) and (b) Model and physical field of small-scale (4.5 × 4.5 cm^2) and large-scale (1 × 2 m^2) devices, respectively, and the red arrows indicate the wind field directions. (c)–(e) Simulated temperature profile of small-scale and large-scale prototypes, and the large-scale pristine PV panel without cooling components.

system demonstrates an increase in electricity generation of up to 7.5%. The experimental and simulation results indicate that it is a promising approach to fulfill the cooling demand in the PV industry with broad adaptability.

Abbreviations

PV   Photovoltaic
AWH-EC   Atmospheric water harvesting-based evaporative cooling.

Author contributions

The manuscript was written through contributions of all authors. All authors have given approval to the final version of the manuscript.

Conflicts of interest

There are no conflicts to declare.

Acknowledgements

References

1 Global solar capacity additions hit 268 GW in 2022, says BNEF, https://www.pv-magazine.com/2022/12/23/global-solar-capacity-additions-hit-268-gw-in-2022-says-bnef/, (accessed 2023 February 7, 2023).
2 J.-W. Arnulf, *PV Status Report 2019*, Report 978-92-76-12608-9, Luxembourg, 2019.
3 S. Dubey, J. N. Sarvaiya and B. Seshadri, *Energy Procedia*, 2013, **33**, 311–321.
4 E. Skoplaki and J. A. Palyvos, *Sol. Energy*, 2009, **83**, 614–624.
5 S. Rühle, *Sol. Energy*, 2016, **130**, 139–147.
6 W. Wang, S. Aleid, Y. Shi, C. Zhang, R. Li, M. Wu, S. Zhuo and P. Wang, *Joule*, 2021, **5**, 1873–1887.
7 E. Schmidt, *Properties of water and steam in SI-units 4 enlarged ed*, Springer, Germany, 1989.
8 S. Nižetić, E. Giama and A. M. Papadopoulos, *Energy Convers. Manage.*, 2018, **155**, 301–323.
9 H. Bahaidarah, A. Subhan, P. Gandhidasan and S. Rehman, *Energy*, 2013, **59**, 445–453.
10 *Encyclopedia of Climate and Weather*, ed. S. Schneider, T. Root and M. Mastrandrea, Oxford University Press, 2 edn, 2011.
11 M. A. Al-Tameemi and V. V. Chukin, *J. Atmos Sol. Terr. Phys.*, 2016, **142**, 55–59.
12 L. Bengtsson, *Environ. Res. Lett.*, 2010, **5**, 025202.
13 R. Li, Y. Shi, M. Wu, S. Hong and P. Wang, *Nat. Sustainable*, 2020, **3**, 636–643.
14 R. Li, W. Wang, Y. Shi, A. C.-T. Wang and P. Wang, *Adv. Mater.*, 2023, 2209460.
15 O. M. Yaghi, M. O'Keeffe, N. W. Ockwig, H. K. Chae, M. Eddaoudi and J. Kim, *Nature*, 2003, **423**, 705–714.
16 O. M. Yaghi, *J. Am. Chem. Soc.*, 2016, **138**, 15507–15509.
17 H. Jiang, D. Alezi and M. Eddaoudi, *Nat. Rev. Mater.*, 2021, **6**, 466–487.
18 R. G. AbdulHalim, P. M. Bhatt, Y. Belmabkhout, A. Shkurenko, K. Adil, L. J. Barbour and M. Eddaoudi, *J. Am. Chem. Soc.*, 2017, **139**, 10715–10722.
19 H. Furukawa, F. Gándara, Y.-B. Zhang, J. Jiang, W. L. Queen, M. R. Hudson and O. M. Yaghi, *J. Am. Chem. Soc.*, 2014, **136**, 4369–4381.
20 H. Kim, S. R. Rao, E. A. Kapustin, L. Zhao, S. Yang, O. M. Yaghi and E. N. Wang, *Nat. Commun.*, 2018, **9**, 1191.
21 A. J. Rieth, S. Yang, E. N. Wang and M. Dincă, *ACS Cent. Sci.*, 2017, **3**, 668–672.
22 E. Gkaniatsou, B. Meng, F. Cui, R. Loonen, F. Nouar, C. Serre and J. Hensen, *Nano Energy*, 2021, **87**, 106224.
23 L. Zhu, L. Tian, S. Jiang, L. Han, Y. Liang, Q. Li and S. Chen, *Chem. Soc. Rev.*, 2023, **52**, 7389–7460.
24 S. M. Towsif Abtab, D. Alezi, P. M. Bhatt, A. Shkurenko, Y. Belmabkhout, H. Aggarwal, Ł. J. Weseliński, N. Alsadun, U. Samin, M. N. Hedhili and M. Eddaoudi, *Chem*, 2018, **4**, 94–105.